Pore Surface Fractal Characterization in Waste Cotton-derived Carbon Materials and the Effect of Pyrolysis Conditions on the Level of Sulfonation

Lulu Zhang,[a] Sufeng Zhang,[a,*] Jinfan Yang,[a] Congcong Chi,[a,*] and Qingyi Wang [b]

Waste cotton-derived carbon materials were synthesized using various chemical activators, and their performance as solid acid catalyst supports was studied. The pore surface structures of the carbon materials were quantitatively characterized by surface fractal dimension, and the relationship between pore surface structure and the density of catalyst was also investigated. The pore sizes were grouped into four ranges, including fractal dimensions D_1 (0.32 nm to 2.0 nm) and D_2 (2.0 nm to 50 nm), as revealed by N_2 adsorption and Frenkel-Halsey-Hill fractal theory. In addition, D_3 (50 nm to1000 nm) and D_4 (1000 nm to 200,000 nm) were revealed by mercury intrusion porosimetry and the Friesen-Mikula fractal theory. The surface fractal dimension *D* was found to be proportional to the density of SO_3H groups from sulfonation at the same carbonization temperature. A larger *D* value corresponded to the exposure of more active sites, which was more favorable for improving the density of SO_3H groups. With the rise of carbonization temperature, the surface fractal dimension also increased. However, the graphitization structure of carbon materials increased with the rise of carbonization temperature, which reduced the active sites of SO_3H groups. Finally, the solid acid catalysts prepared *via* the sulfonation process were used in the esterification reaction of levulinic acid and *n*-butanol.

Keywords: Waste cotton products; Carbon materials; Surface fractal dimension; Solid acid catalyst; Esterification reaction

Contact information: a: Shaanxi Provincial Key Laboratory of Papermaking Technology and Specialty Paper Development, National Demonstration Center for Experimental Light Chemistry Engineering Education, Key Laboratory of Paper Based Functional Materials of China National Light Industry, Shaanxi University of Science and Technology, Xian 710021, China; b: Shaanxi Environmental Protection Research Institute Co., Ltd., Xi'an 710077, China;
** Corresponding authors: zhangsufeng@sust.edu.cn; congcongchi@163.com*

INTRODUCTION

Cellulose is one of the most abundant natural polymers on the earth. The natural macromolecular compound containing the highest cellulose content (approximately 90% to 94%) is cotton fiber, which is widely used in cotton textiles. However, many cotton products are unrenewable because of the performance deterioration during use and the high cost of the renewing processes (Kamm 2007). Designing low-cost and high-performance waste cotton product (WCP) -derived materials is the key to promoting their environmental friendliness and economic benefits. Biomass-derived carbon materials have been an appealing topic for decades because of their large specific surface area and adjustable pore structures, and they are widely applied as catalysts and catalyst supports (Suganuma *et al.* 2010; González *et al.* 2017; Zhu *et al.* 2017). Therefore, preparation of

porous carbon materials from direct carbonization of WCPs and their use as catalyst supports is an effective method for the high-value utilization of cotton waste. This process is cheaper and easier than other high-cost methods (Oliveira and Teixeira da Silva 2014; Patil *et al.* 2014).

The specific surface area, pore size, and pore surface structure are important indicators for characterizing the performance of catalyst supports and crucially influence the loading and activity of catalysts (Yan *et al.* 2013; Patil *et al.* 2014). Compared with the other two indicators, however, little attention has been paid to pore surface structure, which is a three-dimensional space and is difficult to measure using traditional geometric methods (Tsakiroglou and Payatakers 2000; Zhang *et al.* 2009). The fractal theory proposed by Mandelbrot (1975) effectively compensates for the shortcomings of traditional geometric methods and is essentially reflective of the characteristics of the surface of porous materials (Li *et al.* 2016). The surface fractal dimension *D* quantifies the irregularities of pore surfaces and by definition ranges from 2 (smooth surface) to 3 (surface with maximum roughness).

Based on two fractal theories (Fu *et al.* 2017), the surface fractal dimensions can be calculated from N_2 adsorption data and mercury intrusion porosimetry (MIP) data. The Frenkel-Halsey-Hill (FHH) model, based on N_2 gas adsorption isotherms, has proven to be the most effective method for calculating the pore surface fractal dimension when the pore diameter is less than 50 nm (Jaroniec *et al.* 1997; Chi *et al.* 2017). The surface fractal dimension of large pores (> 50 nm) has been calculated using the Friesen-Mikula mathematical model based on MIP data (Friesen and Mikula 1987; Mahamud 2006). In this study, D_1, D_2, D_3, and D_4 correspond to the unitless fractal dimensions for pore-sizes of 0.32 nm to 2.0 nm, 2.0 nm to 50 nm, 50 nm to 1000 nm, and 1000 nm to 200,000 nm, respectively.

Herein, WCP-derived carbon materials with various pore surface structures were prepared using $ZnCl_2$ and $KHCO_3$ as activators. Then, the SO_3H group was introduced by direct sulfonation on the carbon materials to form solid acid catalysts. The surface fractal dimension *D* of the carbon materials in each of the four ranges was first calculated using the two fractal theories. Second, the relationship between *D* and the SO_3H content was determined. Finally, the solid acid catalysts were used in the esterification reaction between levulinic acid (LA) and *n*-butanol. This research aims to provide a new design idea for other catalyst supports.

EXPERIMENTAL

Materials

The WCPs (Qinglong Textile Mill, Xi'an, Shaanxi, China) refer to the waste fabric produced during the textile process; they were washed, dried, and broken into short fiber dimensions for use. The preparation process of the cotton textile thread used therein is: the cotton is prepared into a cotton textile thread through a process of cleaning, carding, combing, spinning, *etc*., and without removal of waxes. Levulinic acid (LA), *n*-butanol (Aladdin Chemicals, China), $ZnCl_2$, and $KHCO_3$ (Kermel, Germany) were also used. Deionized water was used in all experiments.

Preparation of Carbon Materials

Typically, a specific amount of activator ($ZnCl_2$ or $KHCO_3$) was dissolved in 40 mL of deionized water, and then 2 g of WCPs was added to the solution. The mixture was then heated to approximately 105 °C in a tubular furnace at a rate of 5 °C/min under a nitrogen environment. It was kept at that temperature for 1.0 h to remove moisture. The resulting solutions were then heated at a ramp rate of 10 °C/min to 450 °C or 850 °C, maintained for 3 h, cooled down to room temperature, and boiled for 1.0 h with 100 mL of 1.0 M HCl solution to remove the activators and other impurities. The product was immersed in deionized water, boiled, and then filtered. The solid was repeatedly washed to a neutral pH and dried at 105 °C overnight. Carbon materials without any activator were also prepared under the same conditions for comparison.

Preparation of Solid Acid Catalyst

Approximately 1.0 g of each of the three kinds of carbon materials was mixed with 10 mL of 98% H_2SO_4 (wt%) solution in a hydrothermal reactor for 10 h of sulfonation reaction at 150 °C. After that, the products were washed several times until the washings became neutral, and then they were dried at 105 °C overnight.

The solid acid catalyst were labeled C_{xAyS}, where *x* is the activator:WCP ratio; A is the activator, $ZnCl_2$ (Z) or $KHCO_3$ (K); *y* is the carbonization temperature; and S denotes sulfonation. Preparation Conditions of Some Solid Acid Catalysts are shown in Table 1.

Table 1. Preparation Conditions of Some Solid Acid Catalysts

Sample	Activator	Activator:WCP (g/g)	Carbonization temperature (°C)	Sulfonation
C_{450S}	--	--	450	150°C, 10 h
C_{850S}		--	850	
C_{2Z450S}	$ZnCl_2$	2:1	450	
C_{4Z850S}		4:1	850	
C_{2K450S}	$KHCO_3$	2:1	450	
C_{4K850S}		4:1	850	

Material Characterization

Micropores/mesopores were analyzed by N_2 sorption analysis in an automated gas adsorption system (ASAP2460, Micromeritics Instrument Corp, Atlanta, GA) at -195.65 °C, while macropores were detected by an MIP meter (AutoPore IV 9500, Micromeritics Instrument Corp, Atlanta, GA). Scanning electron microscopy (SEM) (Tescan Vega 3 SBH, Tescan, Brno, Czech) and energy dispersive spectrometry (EDS) (Tescan Vega 3 SBH, Tescan, Brno, Czech) were also used. Fourier transform infrared (FTIR) spectra were recorded on an infrared spectrometer from 4000 cm^{-1} to 400 cm^{-1} (Vertex 70, Bruker, Karlsruhe, Germany). The sulfur content in the solid acid catalysts was detected using an elemental analyzer (Vario El Iii, Elementar Analysensysteme GmbH, Langenselbold, Germany). The liquid product butyl levulinate (BL) was analyzed using a gas chromatograph (GC-2014, Shimadzu, Kyoto, Japan) equipped with a flame ionization detector (FID).

Surface Fractal Dimension from N_2 Adsorption Isotherms

The FHH model can be described as shown in Eq. 1:

$$\ln V = C + A \times \ln[\ln(\frac{P_0}{P})] \quad (1)$$

where V (cm^3/g) denotes the volume of adsorbed gas; C is a constant; A represents the slope of the plot of ln V *vs.* ln (ln P_0/P); P_0 (MPa) denotes the saturation pressure of adsorbed gases; and P (MPa) represents the equilibrium pressure.

The solid-gas potential controls the adsorption process during the early multilayer formation, so the fractal dimension D (nm) can be computed as follows:

$$D = 3(A+1) \quad (2)$$

The interface is controlled by liquid-gas surface tension forces, where D should be calculated as follows:

$$D = A+3 \quad (3)$$

Surface Fractal Dimension from Mercury-Injection Curves

The Friesen-Mikula mathematical model can be described as shown in Eq.4:

$$\ln(\frac{dV}{dP}) = (D-4)\ln P \quad (4)$$

where V (cm^3/g) represents the cumulative injection volume at a given pressure, P (MPa) denotes the absolute injection pressure, and D (nm) indicates the fractal dimension of pores.

Catalytic Activity

First, 1.16 g of LA and 4.44 g of *n*-butanol (at a molar ratio of 1:6) were mixed in a reactor to begin the esterification reaction. Then, 0.116 g of catalyst was used with a loading of 10 wt% based on the mass of LA. The esterification reaction proceeded in a hydrothermal reactor for 3 h at a stirring rate of 200 rpm at 100 °C. Then, the reactor was rapidly cooled down in cold water. The product yield was calculated using Eq. 5,

$$X_{BL} = BL/(LA_0 \times 1.4827) \times 100 \quad [\%, mol/mol] \quad (5)$$

where X_{BL} indicates the BL yield; BL indicates the final concentration of BL; and LA_0 denotes the initial concentration of LA.

RESULTS AND DISCUSSION

Microstructures of Carbon Materials

The microstructures of WCP and WCP-derived carbon materials were analyzed using SEM, N_2 adsorption isotherms, and MIP methods. The WCP fibers were linear, with a diameter range of 10 μm to 20 μm, and had a hollow structure (Fig. 1a). After direct carbonization, C_{450} retained its original state (Fig. 1b). When $ZnCl_2$ was used as an activator, the morphologies of both C_{2Z450} and C_{4Z450} appeared as irregular blocks without any noticeable pores (Figs. 1c and 1d) (Xia *et al.* 2016). With $KHCO_3$ as the activator, C_{2K450} and C_{4K450} both displayed three-dimensional and interconnected porous structures

(Figs. 1e and 1f) (Deng *et al.* 2016). Due to the less amount of $KHCO_3$ used in C_{2K450}, it cannot be completely in contact with WCP, so some fiber morphology are retained.

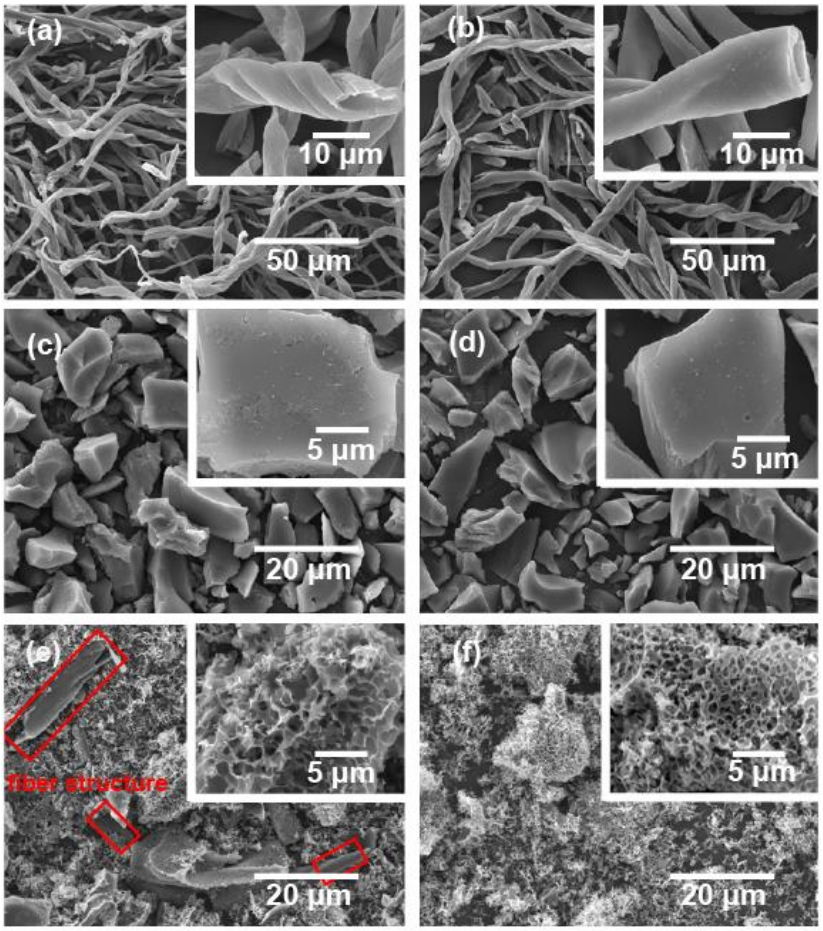

Fig. 1. Morphology evaluation of waste cotton fiber after carbonization with or without activator. SEM images of waste cotton fiber (a) before and (b) after direct carbonization. SEM images of (c) C_{2Z450}, (d) C_{4Z450}, (e) C_{2K450}, and (f) C_{4K450}

Further microstructure analysis showed that the specific surface area and pore volume of C_{450} were small (Table 2), indicating that only the hollow fiber structure remained after carbonization, and no other pore structure appeared. With the use of $ZnCl_2$ as the activator, C_{2Z450} and C_{4Z450} both displayed a large specific surface area, consisting primarily of mesopores, with few micropores or macropores. With $KHCO_3$ as the activator, C_{2K450} and C_{4K450} both had a relatively small specific surface area, which primarily consisted of macropores, with few micropores or mesopores. After carbonization at 850 °C, the specific surface area and pore volume of C_{850} increased compared with C_{450} because more gas molecules were present and more porous structures were thus formed at high temperature. Compared with C_{Z450}, C_{Z850} has a smaller specific surface area and larger pore volume, which was due to the collapse of small pores and the formation of more large pores at high temperature. Compared with C_{K450}, the specific surface area and micropore number of C_{K850} noticeably increased. This was because the CO_2 and H_2O molecules formed from $KHCO_3$ decomposition at high temperature can further react with carbon to form more micropores (Deng *et al.* 2016).

Table 2. BET, Pore Volume, and TPA of Carbon Materials

Sample	BET[a] (m^2/g)	P/P_0[b]:0-0.4 (0.32 nm to 2 nm)	P/P_0[c]:0.4-0.98 (2 nm to 50 nm)	TPA[f] (m^2/g)	P[g]:0.029-0.261 MPa (50 nm to 1000 nm)	P[h]:1.45×10^{-4}-0.029 MPa (1000 nm to 200,000nm)
		*V*mic[d](cm^3/g)	*V*mes[e](cm^3/g)		*V*mac1[i](cm^3/g)	*V*mac2[i](cm^3/g)
C_{450}	16.18	0.004	0.006	0.86	0.001	0.136
C_{2Z450}	2150.61	0.051	0.568	0.08	0.007	0
C_{4Z450}	2046.35	0.023	0.456	0.11	0.003	0
C_{2K450}	207.88	0.075	0.015	16.54	0.965	2.589
C_{4K450}	385.14	0.138	0.028	21.17	1.382	3.622
C_{850}	437.58	0.076	0.033	2.05	0.036	0.587
C_{2Z850}	1786.59	0.147	0.699	1.83	0.151	0
C_{4Z850}	1866.12	0.113	0.701	1.01	0.163	0
C_{2K850}	1189.16	0.421	0.049	43.85	1.986	4.326
C_{4K850}	1522.32	0.650	0.063	65.32	3.287	6.832

a: Brunauer-Emmett-Teller (BET) surface areas were calculated according to N_2 adsorption data; b, c: The relationship of pore width and P/P_0 was calculated by Kelvin's formula; d: Calculated by t-Plot method for micropore analysis; e: Calculated by Barrett-Joyner-Halenda (BJH) method for mesopore analysis; f: total pore area (TPA) computed according to MIP data; g, h: according to the correspondence between pore width and *P*; and i: calculated by MIP for macropore analysis

Effects of Activators and Carbonization Temperature on Pore Surface Fractal Dimension

The plots of ln (ln P_0/P) *versus* ln *V* for carbon materials are shown in Fig. 2. The FHH fractal results show a demarcation point at ln (ln P_0/P) = -0.4, which was utilized to divide the pore diameter into two stages (corresponding to a pore diameter of ~2 nm). At ln (ln P_0/P) > -0.4, A_1 is mostly influenced by multiple layer coverage and monolayer coverage, so D_1 was calculated as $3(A_1+1)$. At ln (ln P_0/P) < -0.4, A_2 is mostly affected by capillary condensation, so D_2 was computed as A_2+3.

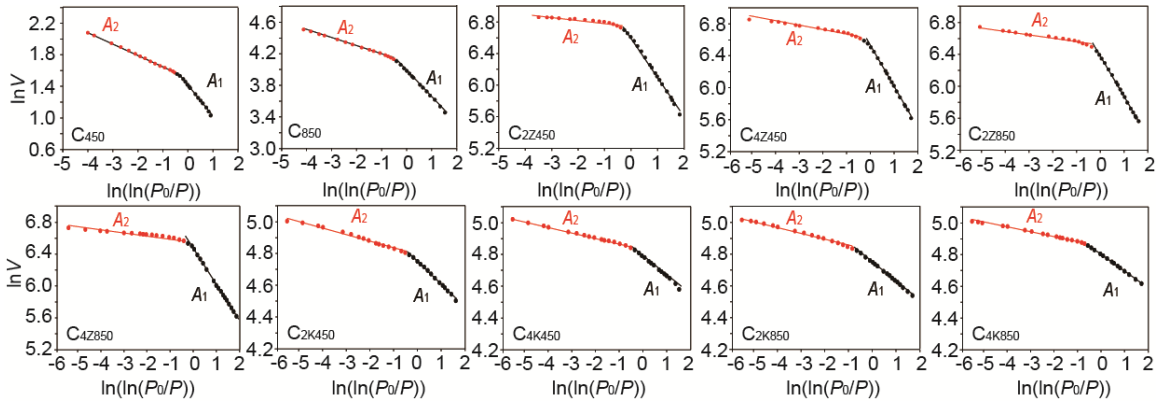

Fig. 2. Plots of ln (ln P_0/P) *versus* ln *V* for carbon materials

Table 3. Fractal Dimension of Microporous and Mesoporous Carbon Materials

Sample	P/P_0:0-0.4 (0.32 nm to 2 nm)				P/P_0:0.4-0.98 (2 nm to 50 nm)		
	A_1	D_1=3(A_1+1)	D_1=A_1+3	R^2	A_2	D_2=A_2+3	R^2
C_{450}	-0.7925	0.6225	2.2075	0.9811	-0.1496	2.8504	0.9961
C_{2Z450}	-0.6189	1.1433	2.3811	0.9918	-0.0760	2.9240	0.9822
C_{4Z450}	-0.6644	1.0068	2.3356	0.9813	-0.1068	2.8932	0.9890
C_{2K450}	-0.2808	2.1576	2.7192	0.9801	-0.0644	2.9356	0.9845
C_{4K450}	-0.1458	2.5626	2.8542	0.9855	-0.0408	2.9592	0.9965
C_{850}	-0.7546	0.7362	2.2454	0.9862	-0.1180	2.8820	0.9868
C_{2Z850}	-0.5371	1.3887	2.4629	0.9870	-0.0433	2.9567	0.9938
C_{4Z850}	-0.5867	1.2399	2.4133	0.9923	-0.0968	2.9032	0.9865
C_{2K850}	-0.1964	2.4108	2.8636	0.9935	-0.0308	2.9692	0.9933
C_{4K850}	-0.0822	2.7534	2.9178	0.9965	-0.0211	2.9789	0.9899

However, the fractal dimension calculated from "D_1=A_1+3" was between 2 and 3, whereas that computed from "D_1=3(A_1+1)" was less than 2, which strays from the definition of the fractal dimension (Table 3). Therefore, the equation "D_1=A_1+3" was used here because it returned more believable values. Analysis of pore surface fractal dimension shows that fractal dimensions D_1 and D_2 of C_{K450} were larger than those of C_{Z450} and C_{450}, at almost 3. This revealed that C_{K450} had very rough pore surface in the range of 0.32 nm to 50 nm; C_{Z450} displayed a relatively smooth pore surface, and direct carbonization formed the smoothest pore surface. These results suggest that the addition of activators can effectively roughen the surface of carbon materials, and the use of $KHCO_3$ maximized the pore fractal dimensions. Meanwhile, the amount of activator also noticeably affected the fractal dimensions. When the amount of $ZnCl_2$ was increased from 1:2 to 1:4, the fractal dimension decreased slightly. This was because excessive $ZnCl_2$ during carbonization hinders the formation of pore structures, resulting in the reduction of specific surface area, pore volume, and pore fractal dimension. When the amount of $KHCO_3$ was 1:2, the insufficient $KHCO_3$ could not fully contact the raw materials, which retained some of the raw materials in the fiber state, thereby reducing the pore surface roughness.

The increasing carbonization temperature effectively increased the pore surface fractal dimension. With increased temperature, some of the original micropores in the carbon materials collapse to form mesopores or macropores. At the same time, the carbon materials further remove oxygen and hydrogen element to form more micropores, which makes the pore structure more complicated.

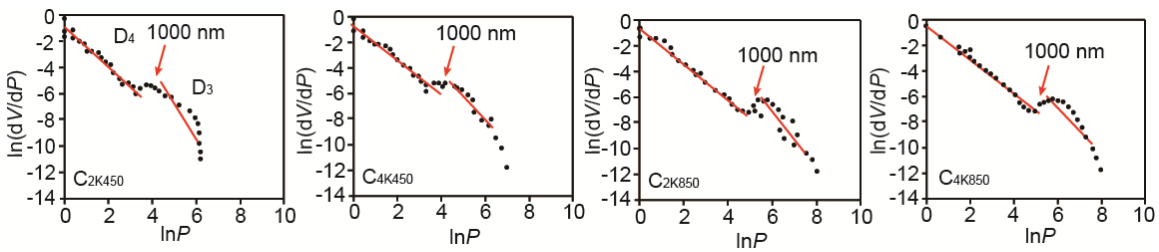

Fig. 3. Plots of ln (d*V*/d*P*) *versus* ln *P* for carbon materials

Table 4. Fractal Dimension of Macroporous Carbon Materials

Sample	*P*: 0.029-0.261 MPa (50 nm to 1000 nm)		*P*:1.45×10^{-4}-0.029 MPa (1000 nm to 200,000 nm)	
	D_3	R^2	D_4	R^2
C_{450}	--	--	--	--
C_{2Z450}	--	--	--	--
C_{4Z450}	--	--	--	--
C_{2K450}	1.8983	0.8154	2.4590	0.9332
C_{4K450}	2.1138	0.8989	2.5255	0.9468
C_{850}	--	--	--	--
C_{2Z850}	--	--	--	--
C_{4Z850}	--	--	--	--
C_{2K850}	2.2553	0.7956	2.6245	0.9511
C_{4K850}	2.5598	0.8014	2.6542	0.9641

The carbon materials C and C_Z had fewer macropores, which did not satisfy the fractal dimension calculation condition. This study reported the macroporous fractal dimension of carbon materials when $KHCO_3$ was used as activator. The plots of ln *P versus* ln (d*V*/d*P*) for C_K are shown in Fig. 3. Linear fitting of the figure suggests that when the pore-diameter range was 50 nm to 1000 nm, the linear relationship was poor ($R^2 < 0.9$). However, when the pore-diameter range was 1000 nm to 200,000 nm, the linear relationship was good (Table 4). This was because at high pressure, the carbon samples were compressed, which did not meet the fractal characteristics under natural conditions (Mahamud *et al.* 2003). Consequently, the fractal dimension *D* calculated from C_K was valid only in the diameter range of 1000 nm to 200,000 nm. Similar to D_1 and D_2, D_4 was also affected by the activator dosage and the carbonization temperature, as a higher carbonization temperature and a larger activator dosage would increase the pore surface fractal dimension.

Relationship between Pore Surface Fractal Dimension and the Density of SO_3H Groups

The morphology of carbon materials after sulfonation and S element maps are shown in Fig. 4.

Table 5. Pore Surface Fractal Dimension, S Content, and SO_3H Density

Sample	SSA[a] (m^2/g)	D_1	D_2	D_4	S content[b] (wt%)	SO_3H density[c] (mmol/g)
C_{450S}	17.04	2.2075	2.8504	--	1.159	0.362
C_{2Z450S}	2150.69	2.3811	2.9240	--	2.803	0.876
C_{4Z450S}	2046.46	2.3356	2.8932	--	2.653	0.829
C_{2K450S}	224.42	2.7192	2.9356	2.4590	3.512	1.098
C_{4K450S}	406.31	2.8542	2.9592	2.5255	3.966	1.239
C_{850S}	439.63	2.2454	2.8820	--	0.732	0.229
C_{2Z850S}	1788.42	2.4629	2.9567	--	1.791	0.660
C_{4Z850S}	1867.13	2.4133	2.9032	--	1.444	0.451
C_{2K850S}	1233.01	2.8636	2.9692	2.6245	2.688	0.840
C_{4K850S}	1587.64	2.9178	2.9789	2.6542	2.782	0.869

a: Specific surface area= BET+TPA; b: Estimated by element analysis; and c: Calculated from S content.

The morphology did not obviously change after sulfonation, suggesting that sulfonation does not noticeably affect the pore structure of carbon materials. According to the S element maps, the SO_3H group was uniformly distributed on the surface of carbon materials.

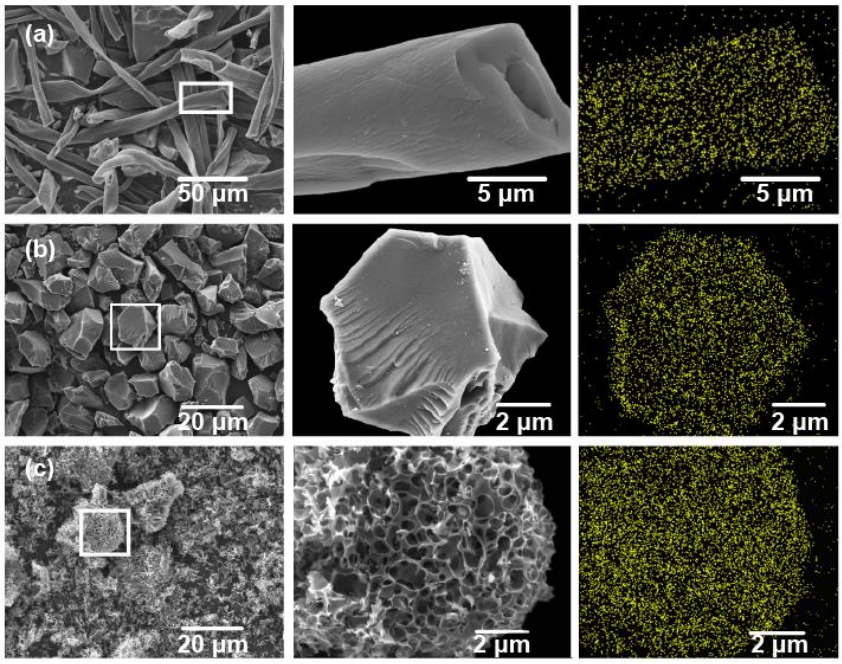

Fig. 4. SEM and S element maps of (a) C_{450S}, (b) C_{2Z450S}, and (c) C_{4K450S}

The relationship between *D* and the density of SO_3H groups is shown in Table 5. After carbonization at 450 °C, the fractal dimension *D* was proportional to the SO_3H density, as a larger *D* corresponds to higher SO_3H density. This result indicates that the higher pore surface fractal dimension and the exposure of more active sites on surface were thus beneficial to improve the density of SO_3H groups. The schematic is shown in Fig. 5.

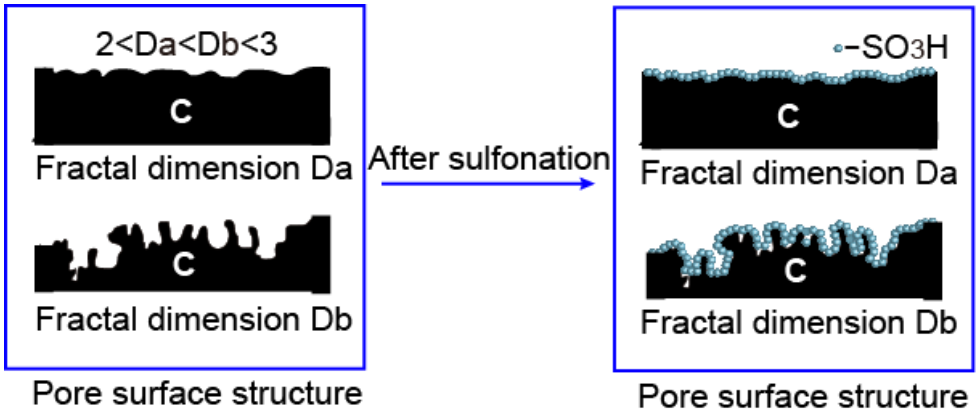

Fig. 5. Schematic of relationship between pore surface fractal dimension and the density of SO_3H groups

After carbonization at 850 °C, the *D* value was still proportional to the SO_3H density and was higher than that for carbonization at 450 °C. However, the density of SO_3H groups decreased. This was because of the excessively high carbonization temperature, which increased the crystallinity of the carbon materials, enlarged the carbon sheets, and thereby reduced the active sites for SO_3H groups (Ma *et al.* 2014). In addition, no direct relationship was found between the specific surface area and the density of SO_3H groups, which is consistent with a previous report (Ma *et al.* 2014).

Application of Solid Acid Catalysts

The carbon-based materials thus prepared were used as solid acid catalysts for the esterification reaction between LA and *n*-butanol. C_{4K450S} displayed the highest esterification yield, 92% (Fig. 6), which was attributed to its highest density of SO_3H groups and its macroporous structure, which facilitated contact between the reactants and SO_3H. C_{850S} showed the lowest esterification yield, 14%, because it had the lowest density of SO_3H groups. Although the SO_3H densities in C_{2Z450S} and C_{4K850S} were similar, their activities were very different. The densities of -COOH and phenolic -OH support groups on the surface of carbon materials decreased with increasing carbonization temperature (Yang *et al.* 2018), which further reduced the synergistic use of -COOH and -OH with SO_3H and thereby decelerated the esterification rate of C_{4K850S} compared with C_{2Z450S}.

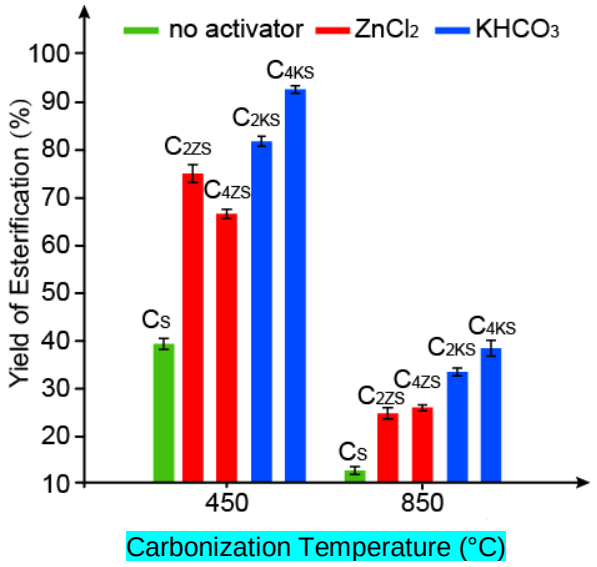

Fig. 6. Carbon-based solid acid catalysts for esterification between levulinic acid and n-butanol

CONCLUSIONS

1. Activators effectively increased the surface fractal dimension *D* of biomass-derived carbon materials. Compared with $ZnCl_2$, $KHCO_3$ as an activator resulted in an increase in *D*, which can be regarded as favorable.
2. At the same carbonization temperature (450 °C or 850 °C), the dimension value *D* was directly proportional to the density of SO_3H groups.

3. Increasing the carbonization temperature increased the surface fractal dimension *D*. However, as the carbonization temperature increased, the crystallinity of carbon materials became less conducive to increase the density of SO_3H groups.
4. The density of SO_3H groups on the surface of solid acid catalysts depends on the pore surface fractal dimension, carbonization temperature, and specific surface area. These factors are interrelated and mutually influential. In addition, one cannot conclude that the density of SO_3H groups is directly related to the specific surface area.

ACKNOWLEDGMENTS

We acknowledge the financial support from the projects of the International Joint Research Center for Biomass Chemistry and Materials, Shaanxi International Science and Technology Cooperation (2018GHJD-19), National Natural Science Foundation of China (31600476), Natural Science Foundation Research Project of Shaanxi Province (2017JQ2015), and Key Scientific Research Plan (Key Laboratory) of Shaanxi Provincial Education Department (17JS016).

REFERENCES CITED

Chi, C., Hui, Z., Liu, M., Zhang, S., and Gong, Y. (2017). "Effect of acetic acid pretreatment on wood pore structure and fractal dimension," *BioResources* 12(2), 3905-3917. DOI: 10.15376/biores.12.2.3905-3917

Deng, J., Xiong, T., Wang, H., Zheng, A., and Wang, X. (2016). "Effects of cellulose, hemicellulose, and lignin on the structure and morphology of porous carbons," *ACS Sustain. Chem. Eng.* 4, 3750-3756. DOI: 10.1021/acssuschemeng.6b00388

Friesen, W., and Mikula, R. (1987). "Fractal dimensions of coal particles," *J. Colloid. Interf. Sci.* 120(1), 263-271. DOI: 10.1016/0021-9797(87)90348-1

Fu, H., Tang, D., Xu, T., Xu, H., Tao, S., Li, S., Yin, Z., Chen, B., Zhang, C., and Wang, L. (2017). "Characteristics of pore structure and fractal dimension of low-rank coal: A case study of lower Jurassic Xishanyao coal in the southern Junggar basin, NW China," *Fuel* 193(1), 254-264. DOI: 10.1016/j.fuel.2016.11.069

González, M., Cea, M., Reyes, D., Romero-Hermoso, L., Hidalgo, P., Meier, S., Benito, N., and Navia, R. (2017). "Functionalization of biochar derived from lignocellulosic biomass using microwave technology for catalytic application in biodiesel production," *Energ. Convers. Manage.* 137(1), 165-173. DOI: 10.1016/j.enconman.2017.01.063

Jaroniec, M., Kruk, M., and Olivier, J. (1997). "Fractal analysis of composite adsorption isotherms obtained by using density functional theory data for argon in slit-like pores," *Langmuir* 13(5), 1031-1035. DOI: 10.1021/la9505529

Kamm, B. (2007). "Production of platform chemicals and syngas from biomass," *Angew. Chem. Int. Ed.* 46(27), 5056-5058. DOI: 10.1002/anie.200604514

Li, A., Ding, W., He, J., Dai, P., Yin, S., and Xie, F. (2016). "Investigation of pore structure and fractal characteristics of organic-rich shale reservoirs: A case study of Lower Cambrian Qiongzhusi formation in Malong block of eastern Yunnan Province, South China," *Mar. Pet. Geol.* 70, 46-57. DOI: 10.1016/j.marpetgeo.2015.11.004

Ma, H., Li, J., Liu, W., Cheng, B., Cao, X., Mao, J., and Zhu, S. (2014). "Hydrothermal preparation and characterization of novel corncob-derived solid acid catalysts," *J. Agric. Food Chem.* 62(23), 5345-5353.DOI: 10.1021/jf500490m

Mahamud, M. M. (2006). "Textural characterization of active carbons using fractal analysis," *Fuel Process Technol.* 87(10), 907-917. DOI: 10.1016/j.fuproc.2006.06.006

Mahamud, M., López, Ó., Pis, J., and Pajares, J. (2003). "Textural characterization of coals using fractal analysis," *Fuel Process Technol.* 86(81), 127-142. DOI: 10.1016/j.fuproc.2004.01.001

Mandelbrot, B. B. (1975). *Les objects fractals: Hazard et dimension*, Flammarion, Paris, France.

Oliveira, B., and Teixeira da Silva, V. (2014). "Sulfonated carbon nanotubes as catalysts for the conversion of levulinic acid into ethyl levulinate," *Catal. Today* 234(1), 257-263. DOI: 10.1016/j.cattod.2013.11.028

Patil, C., Niphadkar, P., Bokade, V., and Joshi, P. (2014). "Esterification of levulinic acid to ethyl levulinate over bimodal micro–mesoporous H/BEA zeolite derivatives," *Catal. Commun.* 43(5), 188-191. DOI: 10.1016/j.catcom.2013.10.006

Suganuma, S., Nakajima, K., Kitano, M., Yamaguchi, D., Kato, H., Hayashi, S., and Hara, M. (2010). "Synthesis and acid catalysis of cellulose-derived carbon-based solid acid," *Solid State Sciences* 12(6), 1029-1034. DOI: 10.1016/j.solidstatesciences.2010.02.038

Tsakiroglou, C., and Payatakers, A. (2000). "Characterization of the pore structure of reservoir rocks with the aid of serial sectioning analysis, mercury porosimetry and network simulation," *Adv. Water Resour.* 23(7), 773-789. DOI: 10.1016/S0309-1708(00)00002-6

Xia, D., Tan, F., Zhang, C., Jiang, X., Chen, Zheng, Li, H., Zheng, Y., Li, Q., and Wang, Y. (2016). "$ZnCl_2$-activated biochar from biogas residue facilitates aqueous As(III) removal," *Appl. Surf. Sci.* 377(30), 361-369. DOI: 10.1016/j.apsusc.2016.03.109

Yan, K., Wu, G., Wen, J., and Chen, A. (2013). "One-step synthesis of mesoporous $H_4SiW_{12}O_{40}$-SiO_2 catalysts for the production of methyl and ethyl levulinate biodiesel," *Catal. Commun.* 34(5), 58-63. DOI: 10.1016/j.catcom.2013.01.010

Yang, J., Li, G., Zhang, L., and Zhang, S. (2018). "Efficient production of n-butyl levulinate fuel additive from levulinic acid using amorphous carbon enriched with oxygenated groups," *Catalysts* 8, 14-25. DOI: 10.3390/catal8010014

Zhang, S., Tang, S., Tang, D., Yan, Z., Zhang, B., and Zhang, J. (2009). "Fractal characteristics of coal reservoir seepage pore, east margin of Ordos Basin," *J. China Univ. Min. Technol.* 38(5), 713-718. DOI: 10.4028/www.scientific.net/AMM.58-60.1701

Zhu, J., Gan, L., Li, B., and Yang, X. (2017). "Synthesis and characteristics of lignin-derived solid acid catalysts for microcrystalline cellulose hydrolysis," *Korean J. Chem. Eng.*, 34(1), 110-117. DOI: 10.1007/s11814-016-0220-5

Article submitted: February 1, 2019; Peer review completed: May 26, 2019; Revised version received: June 20, 2019; Accepted: June 21, 2019; Published: June 28, 2019.
DOI: 10.15376/biores.14.3.6633-6644